RECIPROCAL SPACE XRD MAPPING WITH VARIED INCIDENT ANGLE AS A PROBE OF STRUCTURE VARIATION WITHIN SURFACE DEPTH*

X. Zhao[#], C. E. Reece, Thomas Jefferson National Accelerator Facility, Newport News, Virginia 23606, USA

F. Williams, Q. Yang, Norfolk State University, Norfolk, Virginia 23504, USA

M. Krishnan, AASC, San Leandro, CA 94577, USA

Abstract

In this study, we used a differential-depth X-Ray diffraction Reciprocal Spacing Mapping (XRD RSM) technique to investigate the crystal quality of a variety of SRF-relevant Nb film and bulk materials. By choosing different X-ray probing depths, the RSM study successfully revealed evolution of the materials' microstructure after different materials processes, such as energetic condensation or surface polishing. The RSM figures clearly show the materials' crystal quality at different thickness. Through a novel differential-depth RSM technique, this study found: I. for a heteroepitaxy Nb film Nb(100)/MgO(100), the film thickening process, via a cathodic arc-discharge Nb ion deposition, created a near-perfect single crystal Nb on the surface's top-layer; II. for a mechanically polished single-crystal bulk Nb material, the microstructure on the top surface layer is more disordered than that in-grain.

INTRODUCTION

Next generation SRF particle accelerators call for revolutionary new materials or new surface treatment processes, in order to be more energy efficient. To design and develop an optimal SRF material process, it is necessary to adopt new analytic techniques to non-destructively characterize the SRF functional layer less than 200 nm into the surface. One is interested to understand the crystal quality of the superconductor within this depth.

The definition and measurement of crystal quality in this text is based on crystallographic long-range-order (coherence) of atoms, but not on chemical impurities. As was pointed out by Cullity et al. [1, 2], the quality of so-called "single crystals" or grains, varies from one case to another. At one extreme, a grain might have gone through plastic deformation, such that some portions (subgrains) of the grain are misoriented from the others, thus the dislocation density is high; at the other extreme, some precisely grown crystals have ultra-low density of dislocations, line/planar imperfections (stacking faults), and their crystal planes in that single grain are flat to less than 10^{-4} degrees over a distance of centimeters. Essentially, a motivation of this study is to quantify the density of intra-grain defects in Nb materials by diffraction techniques. It is known in metallurgy, a subgrain is a portion of a crystal or grain slightly different in orientation from neighboring portions of the same crystal. Usually, neighboring subgrains are separated by low-angle boundaries.

To characterize SRF materials, one convenient choice in the SRF community is the electron backscattering diffraction (EBSD) technique. EBSD has been widely used to investigate the microstructure of SRF Nb materials (thin film or bulk). The probing depth of EBSD is ~ 50 nm, which is comparable to the SRF London penetration depth. Therefore, EBSD measurements have provided useful insights into SRF materials in many studies[3, 4].

A popular choice of the EBSD tool, is a commercial software of the EDAX/TSL[TM] company. The program is called OIM[TM] Data Collections and Analysis. The OIM stands for crystallographic "Orientation Indexing Mapping" of crystals, which is the core-value of a commercially available EBSD toolbox.

The limit of the EBSD technique is that the state-of-art EBSD instrument is mainly applied to visualize orientation of multiple crystals/grain (inter-grains characteristics, grain boundaries angles, grain size etc). A single crystal's quality, or intra-grain's density of structural defects is beyond the primary scope of the OIM technique.

Albeit some works [4] using intra-grain mis-orientation map to plot large strain/stress in a crystal, noticeable, a mis-orientation angle less than 1^0 is difficult to discriminate by EBSD. Note, an XRD measurement could scan in a minimal angle step of 0.003^0 in high resolution mode, or 0.06^0 in reciprocal space mapping measurement.

The width of a Kikuchi band does directly relate to crystal lattice constant. Unfortunately, TSL OIM software does not record or quantify that information. In other words, for EBSD OIM software, there is no tool to measure $\Delta\theta_{hkl}$, or crystal lattice constant deviation.

Only a few indirect parameters in the EBSD OIM[TM] software, such as Confidence Index (C.I.) of grain-orientation indexing/assignment, and Imaging Quality (I.Q.) of a Kikuchi diffraction pattern, which are extracted from the EBSD imaging dataset, might shed qualitative light on intra-grain crystal quality.

To relate our measurements to conventional EBSD mapping techniques, we have presented the measured CI and IQ values as benchmarks.

In short, the EBSD technique has its limitation as a tool for characterizing the individual gains/crystals.

Research on crystal quality is on revealing subtle deviation of crystal planes (e.g. bending, twisting, polygonization) or plane distance (d_{hkl}, which is proportional to the lattice constant). Outside the SRF

community, in scientific research of semiconductors [5-9], macromolecular crystal proteins [2] and optic-electronics [10], the X-ray Diffraction reciprocal space mapping technique (XRD RSM) has been widely utilized, for example to measure the structural properties of epitaxial films, or to reveal film composition, layer tilting, lattice relaxation and crystal quality. Such RSM plots could demonstrate the strain, relaxation, and misorientation of a thin film on a substrate. The detection area of an X-ray machine could be a few square centimeters. In an RSM plot, both $\Delta\theta_{hkl}$ (Lattice Constant deviation) and $\Delta\omega$ (Crystal Planes Misorientation) are observable. Different structural properties maybe revealed in one graph.

Here we describe a novel RSM technique, using X-ray penetration of a sample (film or bulk) to different depths. The depth variation is accomplished by varying the incident angle of the X-rays. Thus this new technique allows nondestructive investigation of a material's structural character at different depths. It can reveal structural evolution of an SRF material after different processes, such as film coating, polishing or heating.

EXPERIMENTAL METHOD

To validate the use of RSM for Nb materials study, three types of representative coupon samples were selected. They went through different materials processes. It is expected that these representatives have distinct microstructure character in surface and in the bulk layer. For this study, the surface thickness of interest is less than one hundred nanometers, because only this depth is relevant to the RF London penetration depth in an SRF application.

Film samples dubbed "CED-34", "CED-38", "CED-47" are Nb films that were coated on single crystal MgO (100) substrates using AASC coaxial energetic deposition (CED) facility. The bulk sample "Nb-SC-01" is a single crystal Nb coupon. Sample "Nb-PC-01" is a polycrystalline bulk Nb coupon.

The AASC deposition method of making film samples has been described elsewhere [11-16]. The energetic condensation was conducted via a cathodic arc-discharge Nb ion deposition.

The bulk Nb coupons "Nb-SC-01" and "Nb-PC-01" (10×10×3 mm), were chemically-mechanically-polished (CMP'ed process) at Wah ChangTM company. The CMP is a "mirror-finishing" process to obtain an ultra-flat surface. After CMP, the samples were lightly chemically etched for a few microns to remove the "damage-layer" that is caused by the mechanical polish. The etch used was the typical "buffered chemical polish" (BCP) applied to niobium. After the BCP process, most of the impurity residuals or crystallographic defects were removed. The surface appeared very shiny and morphologically flat under the SEM.

The Residual Resistance Radio (RRR) values of the Nb film samples were measured at the vertical cryogenic testing area (VTA) of Jefferson Lab. In this study, the RRR value is defined as the ratio of resistivity at 300 K to that at 10 K.

Pole Figure and Reciprocal Space Mapping (RSM) measurements were performed at Norfolk State University, using a high resolution four-circle PANalytical X'Pert Pro Materials Research Diffractometer (Pro-MRD). The system was especially designed for thin film analysis and operated with a Cu Kα X-ray source at a wavelength of 1.54 Å. Unless specified otherwise, the X-ray beam projection area on a sample was 2×2 mm. The incident optics was a high-resolution four bounce Ge(220) monochromator, and the diffraction optics was a High Resolution Triple Axis/Rocking Curve element.

Figure 1 shows a standard XRD experimental arrangement. The angle θ_{hkl} stands for diffraction angle of {hkl} Bragg planes; ω is an X-ray beam incident angle; ϕ is an azimuth angle of the sample stage; ψ is a tilting angle against the normal direction of the sample stage.
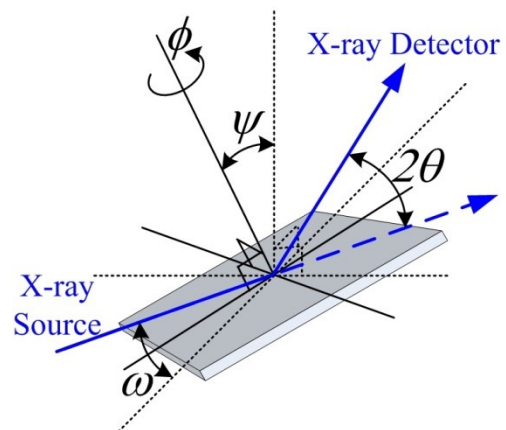

Figure 1: Standard XRD experimental arrangement.

To investigate the FWHM of a single XRD peak, the scan step was set to 0.003^0 to fully use the high resolution of the system. The scan step was changed to 0.01^0 for full range θ-2θ scan, 0.06^0 for reciprocal space mapping measurement, 0.1^0 for ϕ scan and 2^0 for pole figure measurements.

XRD Pole Figure protocol is particularly useful to measure the texture of polycrystalline materials (*aka*. *preferential orientation*), or mis-orientation of a single crystal film against a cut-plane. The principles of pole figure surveys can be found in an X-ray diffraction textbook [1].

In our pole figure measurements, the sample was tilted from $\psi = 0^0$ to 90^0 with a step of 2^0. At each ψ position, the sample was rotated around its normal direction from $\phi = 0^0$ to 360^0 at a step of 2^0 while at the same time the XRD signal was collected by a detector at the fixed $2\theta_{hkl}$ position. For instance, the $2\theta_{110}$ angle is 38.55^0 for detecting the Nb {110} plane. More experimental arrangement in this study was also described elsewhere [12]. Essentially, The XRD pole figure technique uses a "fixed length" of X-ray scattering vector (by lock-in $2\theta_{hkl}$)

to map a family of {*hkl*} points in reciprocal lattice space (*k*-space).

Three samples were surveyed by a Pole Figure measurement. Figure 2 (a-c) are the experimental results of Nb {110} Pole Figures. Fig. 2 (a) is a PF of sample "CED-034". It is the Nb(100) film on MgO (100) substrate. (b) is sample "Nb-SC-01". It is a single crystal bulk Nb (100) coupon. (c) is sample "Nb-PC-01". It is a polycrystalline bulk Nb coupon.

Fig. 2 (a) and (b) demonstrated that the samples are "single crystal". Nb (100) and Nb(110) crystal planes are parallel to substrate cut-surface (*in-plane*) respectively. Fig. 2 (c) confirms that sample "Nb-PC-01" is a polycrystalline material, the grains have no preferential orientation, or no obvious texture.
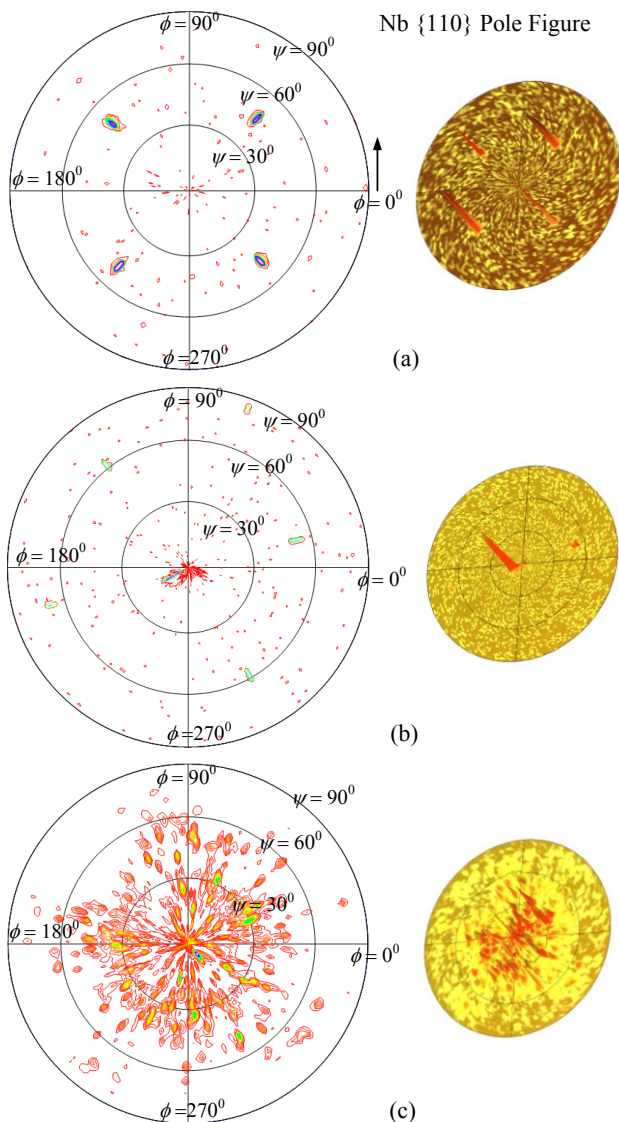

(a)

(b)

(c)

Figure 2: Experimental Nb {110} Pole Figures. (a) Sample CED-034, a Nb(100) film on MgO (100) substrate. (b) Sample Nb-SC-01, a single crystal bulk Nb (110) coupon. (c) Sample Nb-PC-01, a polycrystalline bulk Nb coupon. The right column shows a 3D view of the pole figures.

06 Material studies

I. Basic R&D New materials - Deposition techniques

Reciprocal space mapping was used to characterize intra-grain structures of three samples (Film "CED-34", Bulk "Nb-SC-01" and "Nb-PC-01"). A RSM plot usually shows a distribution of diffraction intensity of one {*hkl*} point in reciprocal space. Structural information of the samples could be interpreted from a profile of the reciprocal lattice point. Experimental RSM data is presented in a two-dimensional " ω vs. $\omega/2\theta$ " plot . The "$\omega/2\theta$" means the machine running under a coupled $\omega/2\theta$ scan mode, *aka* $\theta/2\theta$ (Bragg-Brentano) scan mode. Its *x*-coordinate represents variable θ.

By Bragg's law, $2d_{hkl} \times \sin(\theta_{hkl}) = \lambda_{Cu,K\alpha}$, $\Delta\theta_{hkl}$ is proportional to the distortion of lattice space (Δd_{hkl}) . A broadening effect along the θ_{hkl} coordinate indicates variation in d_{hkl} (spacing of crystal planes {hkl}). d_{hkl} is proportional to the lattice constant (*a*) of Nb, which is a body-centered cubic (BCC) structure, and

$$d_{hkl} = a / \sqrt{h^2 + k^2 + l^2},$$

thus the Nb lattice distortion $\Delta a/a$ (%) can be derived from $\Delta\theta_{hkl}$.

A broadening in ω direction (or $\Delta\omega$) embodies misorientation spread of a {*hkl*} crystal-plane, which implies structural imperfection in the sample (grain) due to "mosaic spread" (evidence of subgrains), dislocations population, bending or polygonization of a lattice.

Before each RSM survey, a {*hkl*} Bragg plane (or θ_{hkl}), a X-ray incident angle (ω_0), an azimuth angle (ϕ), and a sample stage tilting angle (ψ) were selected in order to probe a specific penetration depth in a particular sample. Then, the XRD machine scans in a $\omega/2\theta$ mode at different offset. Scan step of ω or 2θ is 0.06^0 .

To calculate penetration depth (*t*) of an X-ray beam, this equation from Cullity's book is applied [1]:

$$t = \sin\alpha / \mu$$

here α is an incident angle ; $\mu = 1259$ is the absorption coefficient of Nb at $\lambda_{Cu,K\alpha} = 1.54$ Å.

By controlling the penetration depth, we could either investigate the RSM of a surface layer, which is a few hundred nanometers, or probe that of a thicker (includes integration over the surface) layer. By comparison of RSM plots of a thinner layer to that of a thicker layer, one may discriminate the microstructure at different depths. This may reveal the structure evolution of the Nb sample after a coating or polishing.

For a shallow and a thick thickness survey, although different reciprocal points in *k*-space were observed via RSM, it is still reasonable and meaningful to compare profiles of the points. This is because: I. In the same sample measurement, the observed reciprocal points belong to the same {hkl} crystal plane family; II. Nb crystal lattice is a cubic structure, whose symmetry determines that a deviation of one {hkl} shall lead to a proportional deviation of the other {hkl} points, since the volume of a cubic "box" lattice shall be conservative.

Because a strain of the lattice is always three dimensional, while the state-of-art RSM is a two dimension plot of such incoherence lattices, it is unrealistic to apply a 2D graph to depict a 3D lattice.

This is not a problem particular to our RSM study, but a conventional challenge to visualize 3D space structure by XRD.

The EBSD system being utilized in this study, being made by the EDAX/TSL[TM] company, is installed on an Amray[TM] scanning electron microscope (SEM) at Jefferson Lab. The EBSD arrangement is equipped with a TSL-OIM[TM] software to acquire and index the crystallographic orientations.

In this study, two parameters related to crystal quality were recorded for parallel comparison. The abbreviation of "Avg. C.I." means the Average Confidence Index; while "Avg. I.Q." means the average "Image Quality" of the "Kikuchi imaging pattern" (an electron backscattering diffraction pattern). Higher C.I. means the TSL[TM] crystal orientation indexing software has a higher confidence to index the crystal zone and orientation, under that e-beam scan spot. Higher I.Q. means the Kikuchi imaging pattern (being originated at a single e-beam scan spot), is sharper. For a strained zone, then, a spot with a high density of crystallographic defects, has a Kikuchi image quality worse than that of a perfect crystal zone.

RESULTS AND DISCUSSION

Crystal Quality Evolution via Film Thickening

Investigation of a Nb Epitaxy Film at Different Penetration Depths by RSM

In our previous studies[11-16], a trend became obvious that by coating a thicker Nb film, average crystal quality of a single crystal Nb film is advanced, as represented by RRR value, a bulk electrical property.

It was suspected that the crystal quality of a film's top-layer has been progressively improved, as the grains were being continuously thickened (in other words, the grain grows up). To confirm our speculation, we selected two material analysis techniques (RSM and EBSD) to probe the crystal quality of sample Nb films.

Initially, Nb Film sample CED-34 was surveyed by RSM. This film sample was coated by a typical AASC CED[TM] deposition method. Before coating, the magnesium oxide crystal substrate with (100) in plane was annealed at 700 ^{0}C for 12 hours. The substrate temperature was set at 500 ^{0}C during deposition. The Nb film thickness was about 1.6 microns. The RRR value of the sample is 277; the superconducting transition temperature 9.21-9.25 Kelvin.

Through a Pole Figure measurement of Nb {110}, and two "ϕ scans" of Nb {110} and MgO{110} at orbital ψ = 60^0 respectively, the epitaxial relationship between the Nb film and MgO substrate is revealed. It is Nb(100)//MgO(100) with Nb[100]//MgO[110], which was called as Type "O_p" epitaxial relationship in the Hutchinson' study[19, 20].

Table 1 shows two RSM experimental arrangements (1.1 & 1.2) on surveying sample CED-34. Both arrangements probed {123} reciprocal points (by fixing $2\theta_{123}$ = 121.8^0), but at different k-space positions. They have different probing depths.

For arrangement 1.1, the RSM survey probes a shallow surface layer (with penetration depth about 430nm). Figure 3 is the experimental RSM graph of sample CED-034 as described in Table 1.

Table 1: Two RSM Experimental Arrangements to Measure {123} Reciprocal Points at Different X-ray Penetration Depths. Sample label is CED-34. It is a Nb film on MgO (100) substrate.

Experimental Arrangement	1.1	1.2
Omega ω (^{o})	3.1	27.3
2Theta, 2θ (^{o})	121.82	121.87
Psi, ψ (^{o})	0.61	58.32
Phi, ϕ (^{o})	28.45	27.65
X-ray Penetration Depth	shallow, ~430 nm	thick, ~3.65 um
Spread of ω at FWHM, $\Delta\omega$ (^{o})	0.1	0.6
Spread of θ at FWHM, $\Delta\theta$ (^{o})	0.1	0.2

For the set-up 1.2 (high incident angle ω), theoretically the X-ray beam could probe a thicker layer (~3.6 microns if all mass is Nb). Because thickness of the Nb film CED-34 is only 1.6 micron, literally, the X-ray beam had sampled the entire through-thickness of the film.

The deviation of lattice constant (*a*) on the top-surface versus that of the entire layer is:

Δa(top-layer)/Δa(entire film) ~= 0.1/0.2=1/2 .

The crystal misorientation on the top-surface versus that of the entire layer is:

Δω (top-layer)/Δω (entire film) ~= 0.1/0.6=1/6.

Fig. 3 (a) for arrangement 1.1 shows a reciprocal point{123}, whose profile is an oval near-circular-shape. Sampling depth of arrangement 1.1 is shallow, about 430nm. The spread of ω and $2\theta_{123}$ at FWHM, $\Delta\omega$ (^{o}) and $\Delta2\theta$ (^{o}), are both small (~0.1^0). Its shape is similar to a singularity k-space point, which suggests that the surface structure of the film is close to a perfect crystal, if being compared to 2(b).

Fig. 3 (b) for set 1.2 shows a reciprocal pole {123}, whose profile is an asymmetrically elongated bar-shape. Sampling depth of arrangement 1.2 is deep, the full 1.2 um. The image obviously deviates from a k-space singularity point. It suggests that the entire film structure might be "bent" or gradually mis-oriented (spread of ω at FWHM, $\Delta\omega$ = ~ 0.6^0).

By comparing the RSM figure of 3(a) to 3(b), it demonstrated that crystal structure of the top-layer of Nb film CED-34 is superior to that of the average ones, regarding the entire film.
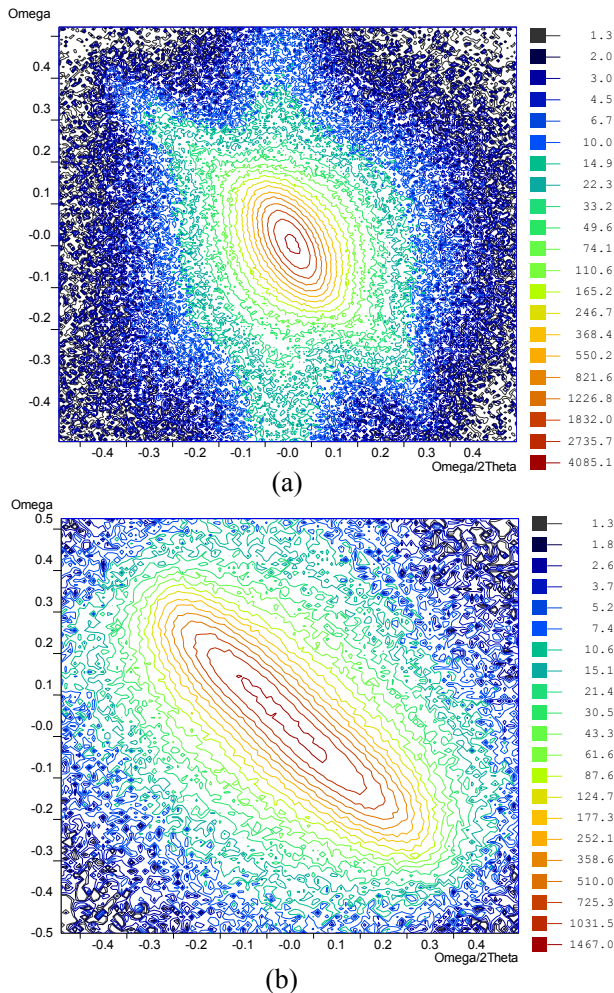

(a)

(b)

Figure 3: RSM experimental plot of Nb film sample CED-034 which are {123} reciprocal points at different X-ray penetration depth. (a) shallow penetration (b) deep penetration.

Investigation of Two Nb Epitaxy Films of Different Thickness by EBSD

To verify whether crystal quality does advance through a film thickening process, the EBSD technique was also applied to measure the crystal quality of two films of different deposition thickness.

The films (CED-47 and CED-38) were created by the same CED deposition conditions as that of CED-34, except their thicknesses are 60 nm and 800 nm, respectively.

Figure 4 shows the samples' EBSD inversed pole figures (IPF). The figures also illustrate thickness difference of the samples. EBSD survey area is 250×250 μm, scan step 10 μm. The IPF graphs grayscale are rendered by I.Q. values, whose rendering scale is [min,max] = [500, 2100]. Bright red color means the

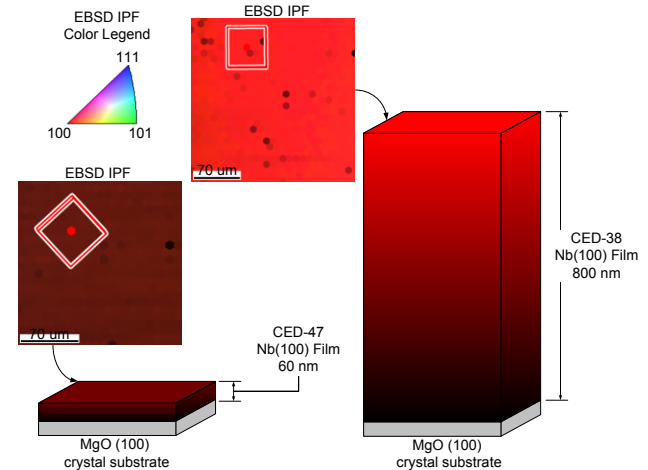scanning zone has a higher crystal quality. Dark red zones are low crystal quality ones

Figure 4: Schematic illustration of Nb Films CED-47 and CED-38. Their surface crystal quality was measured by EBSD. It indicates the Nb film crystal quality progressively evolves by thickening. The square EBSD IPFs are the EBSD inversed pole figures of Nb film sample CED-47 and CED-38. EBSD survey area is 250×250 um, scan step10 um. IPF grayscales are rendered by I.Q. values; Rendering scale is [min,max] = [500, 2100].

Table 2 lists some measurable parameters given by TSL OIM software (being extracted out of the raw data of Fig.4). The table shows the RRR values, an averaged figure of merit to evaluate electrical conductivity, or the electron-mean free path in the state of normal conductivity, increased up from 46 to 136 (~ 3 times) . The superconducting transition temperature (T_c) of the Nb films increased from 8.95 to 9.2K, which also suggested the average crystallographic defect density of Nb film being suppressed via a film thickening.

Table 2: Crystal Quality being measured by EBSD. It shows crystal quality progressively evolves by thickening a Nb film. *C.I. is Confidence Index value; ** I.Q. is Image Quality value

Sample Label	CED-47	CED-38
Thickness (nm)	~60	~ 800
RRR	46	136
T_c (K)	8.95	9.20
Avg. C.I.*	0.67	0.90
Avg. I.Q.**	1121	2101
Avg. Misorientation Angle	0.18^0	0.15^0

The table indicates the average confidence index changes from 0.67 to 0.9; while the average Image Quality has a more obvious change, which is from 1121

to 2101 (about 2 times increment). The average misorientation angle of the scanning area (250 × 250 microns), is smaller than that of the thicker film. But such change (0.18 vs. 0.15) is not obvious. It shows the EBSD technique is not efficient at revealing small misorientation.

Since the probing thickness of EBSD is only about 50nm, and all the EBSD parameters relevant to crystal quality indicated a trend of progression, it substantiated that crystal quality gradually improved as the film thickening progressed. Both RSM and EBSD experiments demonstrated the top layers crystal quality has less crystallographic defect density than that on the interface of the Nb film / MgO substrate.

Investigation of a Single Crystal Bulk Nb Coupon Sample at Different Penetration Depths by RSM

Table 3 shows two RSM experimental arrangements (2.1 & 2.2), which have different probing depths on bulk sample "Nb-SC-01". Both arrangements were probing {110} reciprocal poles (by fixing $2\theta_{110} = 38.5^0$), at different k-space points.

Table 3: Two RSM Experimental Arrangements to Measure {110} Reciprocal Points at Different X-ray Penetration Depth. Sample label is Nb-SC-01. It is a single crystal bulk Nb (100) coupon sample. *minus sign means tilting direction; [#] it is a spread of multiple sub-peaks

Experimental Arrangement	2.1	2.2
Omega ω (^{o})	19.28	20.53
2Theta, 2θ (^{o})	38.551	38.551
Psi, ψ (^{o})	83.2	-8.12*
Phi, ϕ (^{o})	69.34	0
X-ray Penetration Depth	shallow, ~ 310 nm	thick, ~ 2.75 um
Spread of ω at FWHM, $\Delta\omega$ (^{o})	0.6[#]	0.1
Spread of θ at FWHM, $\Delta\theta$ (^{o})	0.2	0.1

Figure 5 shows the experimental RSM graphs of bulk sample "Nb-SC-01". Arrangement 2.1 probes a shallow surface with penetration depth about 310 nm. Figure 5(a) shows multiple peaks at a reciprocal point {110}, whose profile is an asymmetrical, wide-spread, and multi-

centered contour. This RSM plot is far from that of perfect crystal. Such a multiple-peak image might be explained by formation of subgrains on the surface, with each one having a slightly different orientation (misorientation angles ~ 0.1^0). It is known in metallurgy, subgrain is a portion of a crystal or grain slightly different in orientation from neighboring portions of the same crystal. Usually, neighboring subgrains are separated by low-angle boundaries.
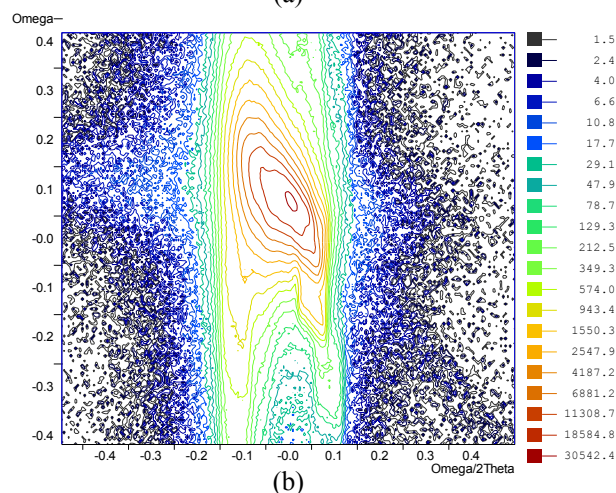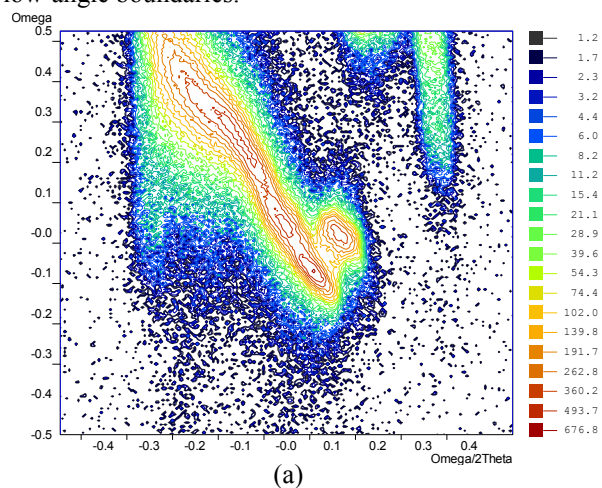

(a)

(b)

Figure 5: Experimental RSM graph of bulk sample Nb-SC-01 as described in Table 3. (a) shallow penetration (b) deep penetration.

The image's obvious deviation from a k-space singularity point suggests that the adopted CMP process plus a light BCP process, still produced a damaged surface structure (strain or subgrains) . The subgrains maybe gradually misoriented (Spread of ω at FWHM, $\Delta\omega$ (^{o}) = ~ 0.6^0).

The set-up 2.2 (high incident angle) probes a thicker layer (2.76 microns if all mass is Nb). Figure 5(b) shows one peak of reciprocal pole {110}, whose profile is in quasi-circular-shape. Its max peak is similar to a singularity k-space point.

The spread of ω and $2\theta_{110}$ at FWHM, $\Delta\omega$ (^{o}) and $\Delta2\theta$ (^{o}), are both small (~0.1^0). Its shape is similar to a singularity k-space point, which suggests that bulk

structure is close to a perfect crystal, if being compared to 5(a).

The deviation of lattice constant (*a*) on top-surface versus that of entire layer is:

Δa(top-layer)/Δa(entire film) ~= 0.2/0.1=2/1 .

The crystal misorientation on the top-surface layer versus that of entire layer is:

Δω (top-layer)/Δω (entire film) ~= 0.6/0.1=6/1.

Thus, the RSM Figure 5 (a) vs. 5(b) demonstrates that the top-layer's crystal structure of the mirror-finished bulk Nb is crystallographically disordered, and top-layer crystal structure is inferior to that of the deep layer, regarding the intra-grain crystal quality.

Investigation of a Polycrystalline Bulk Nb Coupon Sample at Different Penetration Depth by RSM

Table 4 shows two RSM experimental set-ups (3.1 & 3.2), which have different probing depth on bulk sample "Nb-PC-01". Both arrangements were probing {110} reciprocal points (by fixing $2\theta_{110}$ =38.5^0), but at different *k*-space points. Because it is a polycrystalline (with poly-grains) material, it doesn't matter how to set ψ or ϕ angles.

Table 4: Two RSM Experimental Arrangements to Measure {110} Reciprocal Points at Different X-ray Penetration Depth. Sample label is Nb-PC-01. It is a polycrystalline bulk Nb sample.

Experimental Arrangement	3.1	3.2
Omega ω (^{o})	1.5000	19.2755
2Theta, 2θ (^{o})	38.551	38.551
Psi, ψ (^{o})	0	0
Phi, ϕ (^{o})	0	0
X-ray Penetration Depth	shallow, 208 nm	thick, 2.62 um

For arrangement 3.1, the X-ray beam probes a shallow surface (with penetration depth about 208 nm). The X-ray beam sampled the top surface damage layer. Figure 6 presents the experimental RSM graphs as described in Table 4. For the set-up 3.2 (high incident angle), the X-ray beam probes a thicker layer (2.62 microns).

Figure 6 (a) and (b) show similar "stripes" in *k* space, which is a typical sign of poly-grain materials, for the grains are mis-oriented gradually along the ω coordinate. Appearance of (a) and (b) are similar, although the stripe (a) is quite significantly broader in ω direction, and wider in the spread of θ_{110} (in $\omega/2\theta$ coordinate), than that of (b).

As mentioned previously, a broadening effect of θ_{110} implies a larger lattice constant deviation. Intuitively, the plot (a-b) implies that the average crystal quality of deep-layer Nb is better than that of the surface layer, which might still have a damaged area even after being polished. It is hard to describe the difference quantitatively. Nevertheless, such observation of the spread of the "stripe" is consistent with residual surface damage.

Also note, the averaged FWHM width of θ_{110} (in $\omega/2\theta$ coordinate) of Fig. 6(b) is similar to that of 5(b). This suggests that in a deep layer far from the surface the average crystal quality of polycrystalline Nb-PC-01 is comparable to that of the single grain Nb-SC-01.
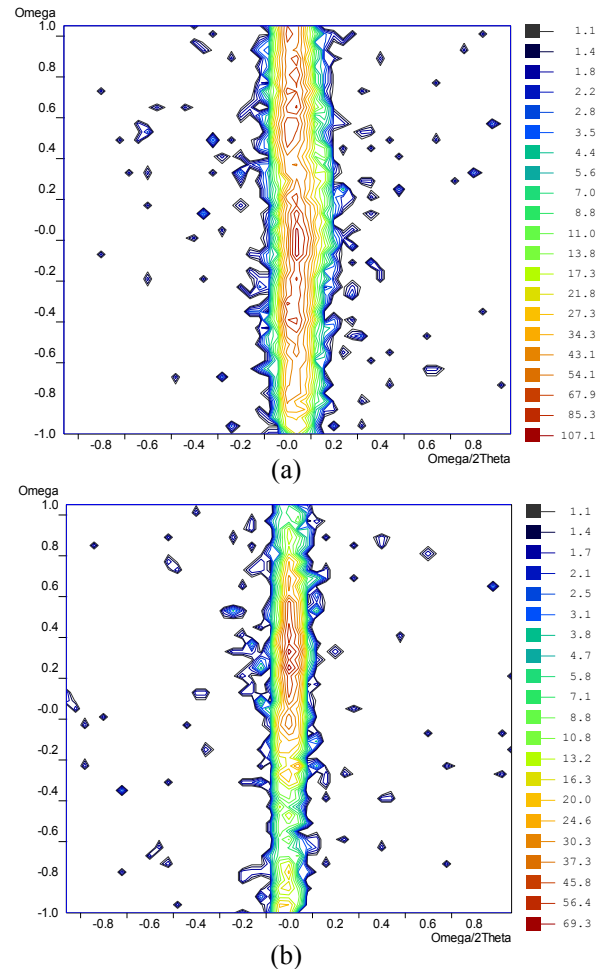

(a)

(b)

Figure 6: The experimental RSM graphs of bulk polycrystalline sample Nb-PC-01 as described in Table 4. (a) shallow penetration (b) deep penetration.

CONCLUSION

We have shown that an XRD RSM measurement is a useful nondestructive technique to measure intra-grain crystal quality of Nb surfaces. By using different X-ray penetration depths, crystal quality at different thickness can be discerned. This technique is efficient and useful to probe SRF materials such as Nb films or bulk single crystal small samples.

This study confirmed that during a Nb film coating process the film thickening process, via energetic deposition, can advance crystal quality of a film's topmost surface-layer, which is of greatest interest for many applications.

For an ultra thin film (say << 50nm) , the microstructural disorder is largely influenced by the interface; by depositing a much thicker film (say, > 1 µm), the topmost layer of 50 nm may obtain a well ordered structure. Such a phenomenon suggests a micron thick film coating shall be suitable for SRF cavities.

The RSM study also confirmed that a mechanical "mirror polishing" introduces substantial microstructure disorders into the bulk Nb material's topmost layer. Chemical polishing or etching is a way to remove the surface damage layer. The particular CMP process plus BCP process used on samples here still left a slightly damaged surface. Process development feedback from the RSM technique described here may guide optimization of optimal surface processing of bulk materials in additions to thin film materials. A very recent study on high temperature treatment of large grain SRF Nb cavity has successfully adopted the RSM and Pole Figure techniques to reveal the surface structure-properties relationship[21].

ACKNOWLEDGMENT

REFERENCES

[1] B. D. Cullity, *Elements of X-Ray Diffraction*. (1978).

[2] E.H. Snell, et al. Macromolecular crystal quality. Methods Enzymol. (2003).

[3] Xin Zhao, et al, Phys. Rev. ST Accel. Beams 13 (12), 124701 (2010).

[4] T. Bieler, etal., Phys. Rev. ST Accel. Beams (2009).

[5] Hiroyuki Yoshida, et al, APPLIED PHYSICS LETTERS 90, 181930 (2007).

[6] A. Tersigni, et al., PHYSICAL REVIEW B 84, 035303 (2011).

[7] J.F. Woitoke et al., International Centre for Diffraction Data 2005, Advances in X-ray Analysis, 48, 165 (2005).

[8] Detlef-M. Smilgies, et al., Journal of Synchrotron Radiation 12, 807–811 (2005).

[9] P. F. Fewster, NEWSLETTER No. 24, December 2000, COMMISSION ON POWDER DIFFRACTION,INTERNATIONAL UNION OF CRYSTALLOGRAPHY (2000).

[10] E. Koppensteiner, et al., J. Appl. Phys. 76 (6), 3489 (1994).

[11] X. Zhao, et al., J. Appl. Phys. 112, 016102 (2012).

[12] X. Zhao, et al. Journal Applied Physics 110, 033523 (2011).

[13] M Krishnan, et al., Supercond. Sci. Technol. (24), 115002 (2011).

[14] X. Zhao, et al., Journal of Vacuum Science & Technology A 27 (4), 620-625 (2009).

[15] M. Krishnan, et al., presented at the 14th International Conference on RF superconductivity (SRF2009), Berlin, Germany, 2009.

[16] M. Krishnan, et al., Physical Review Special Topics - Accelerators and Beams 15, 032001 (2012).

[17] G. Wu, et al, presented at the Proceedings of the 2003 Particle Accelerator Conference., 2003 (unpublished).

[18] V. Randle, in *Electron Backscatter Diffraction in Materials Science*, edited by A. J. Schwartz, M. Kumar and B. L. Adams (Springer, 2000).

[19] T. E. Hutchinson, et al., J. Appl. Phys. 38, 4933 (1967).

[20] Hutchinson, Journal Applied Physics 36 (1), 270 (1964).

[21] G. C. P. Dhakal, et al., Physical Review Special Topics - Accelerators and Beams 16, 13 (2013).